Radiation Effects and Defects in Solids, 1990, Vol. 113, pp. 331-358
Reprints available directly from the publisher
Photocopying permitted by license only

NON-EQUILIBRIUM AGGLOMERATION OF HELIUM-VACANCY CLUSTERS IN IRRADIATED MATERIALS

S. SHARAFAT and N. M. GHONIEM

Mechanical Aerospace and Nuclear Engineering Department, University of California, Los Angeles, Los Angeles, CA 90024

(Received March 3, 1989; in final form October 3, 1989)

Time evolution of non-equilibrium systems, where the probability density is described by a continuum Fokker-Planck (F-P) equation, is a central area of interest in stochastic processes. In this paper, a numerical solution of a two-dimensional (2-D) F-P equation describing the growth of helium-vacancy clusters (HeVCs) in metals under irradiation is given. First, nucleation rates and regions of stability of HeVCs in the appropriate phase space for fission and fusion devices are established. This is accomplished by solving a detailed set of cluster kinetic rate equations. A nodal line analysis is used to map spontaneous and stochastic nucleation regimes in the helium-vacancy (h-v) phase space. Growth trajectories of HeVCs are then used to evaluate the average HeVC size and helium content during the growth phase of HeVCs in typical growth instability regions.

The growth phase of HeVCs is modeled by a continuum 2-D, time-dependent F-P equation. Growth trajectories are used to define a finite solution space in the h-v phase space. A highly efficient *dynamic re-meshing* scheme is developed to solve the F-P equation. As a demonstration, typical HFIR irradiation conditions are chosen. Good agreement between the computed size distributions and those measured experimentally are obtained.

1 INTRODUCTION

The production of helium in structural components exposed to neutron irradiation results in degradation of mechanical properties. Materials employed in fusion devices are subject to three helium generation processes: (1) the (n, α) nuclear reaction in bulk materials, (2) exposure to high fluxes of α-particles resulting in near-surface deposition of helium atoms, and (3) the decay of tritium to ^{3}He in tritium-contaminated materials. Some macroscopic changes can be readily monitored and measured (i.e., volumetric swelling, intergranular embrittlement, and surface blistering). The cause of these changes can be attributed to the formation and growth of helium-filled cavities (bubbles). To model the formation and evolution of these cavities during irradiation, fundamental kinetic processes must be understood. Upon introduction into the bulk material, helium atoms undergo three distinct phases: transport, nucleation, and growth.

1.1 *Transport*

When a helium atom is first placed into the lattice it will occupy an interstitial site. Being virtually insoluble, it causes a high strain field in its vicinity. This leads to rapid diffusion through the lattice until it interacts with defects such as vacancies (vacant lattice sites), self-interstitial atoms (SIAs), dislocation lines, or grain boundaries. During this transport phase, helium atoms undergo random walk until they are "trapped" by defects. Neutron irradiation results in the formation of helium atoms, vacancies, and SIAs. Vacancies offer interstitial helium atoms a high

number of trapping sites. The interactions between the three fundamental defects (vacancies, self-interstitials, and helium atoms) lead to the formation of small clusters of one to three helium atoms and one to three vacancies, with sizes in the 0.2 to 0.4 nm range.

1.2 *Nucleation*

The clusters formed during the transport phase are in a highly non-equilibrium state and are thus very unstable. For example, an SIA can readily replace a trapped helium atom from a vacant site. (The formation energy for a vacancy-SIA pair is around 4.5 eV while the h-v binding energy has been estimated to be about 3.6 eV in nickel.) For helium-filled cavities to grow, stable HeVCs must first nucleate. Estimates for stable HeVCs indicate that between 3 and 10 defects must be involved for the formation of critical HeVCs.[1] Sizes for critical clusters are in the 0.2 to 1 nm range.

1.3 *Growth*

Beyond the nucleation phase, HeVCs are very stable up to temperatures reaching the metal melting point.[2] Thus the next phase of cavity evolution constitutes the growth phase. Growth can be accommodated by accumulating more helium atoms, absorption of vacancies, or by migration and coalescence with other HeVCs. The insolubility of helium atoms in the matrix[2] causes the helium atoms to be trapped inside small clusters ($r < 10$ Å) which reach pressures exceeding fluid–solid phase transition densities (130 Kbar in Al and 500 Kbar in Ni).[3] For these high densities, sophisticated equations of state (EOS) of helium (analytical[4] and numerical[5]) must be used since Van der Waal's gas law is invalid in this regime. Thus, even during the growth phase, the HeVCs are in a non-equilibrium state which precludes the use of classical nucleation theory and growth models.

All three phases of HeVC formation depend on temperature, displacement damage rate, and helium-atom generation levels. At higher temperatures, the mobility of migrating species and the dissociation rate of HeVCs increase. This results in higher nucleation energy barriers which must be overcome for stable cluster formation to occur. Displacement damage induces vacancy supersaturation (ratio of vacancy concentration to thermal equilibrium vacancy concentration). The supersaturation ratio depends on the overall sink strength of the bulk material and the displacement damage rate in displacements per atom per second (dpa/s). The amount of helium produced [expressed as helium-to-dpa ratio (He/dpa)] plays a significant role in the kinetic processes leading to h-v clustering. These clustering kinetic effects have been studied and reported earlier in detail[6]. Some of the relevant findings will be summarized in Section 2.

The objective of this work is to develop a self-consistent solution for the nucleation and evolution phases of h-v clustering. Since the formation of stable HeVCs at high temperatures (> 450°C) and at high He/dpa ratios (> 50) was found to be spontaneous,[7] we have chosen these conditions as a first attempt to model the growth of HeVCs. Spontaneous nucleation refers to the condition of negligible, nucleation energy barriers.

To our knowledge, this work is the first reported attempt to numerically model the evolution of HeVCs by solving a transient 2-D F-P equation which describes both the helium content and the size of growing helium-filled cavities during

irradiation. In Section 2, we summarize our earlier work on the transport and stability of HeCVs. In Section 3, phase-space analysis of nucleation and evolution is given. The proposed clustering model, derived from arguments based on non-equilibrium statistical mechanics, is developed in Section 4. This is followed by a novel numerical solution to the resulting transient, 2-D F-P equation in Section 5. Applications of the model to neutron-irradiated steels are given in Section 6; Conclusions follow in Section 7.

2 TRANSPORT MODEL AND THE STABILITY OF HELIUM-VACANCY CLUSTERS

Under irradiation conditions, three features complicate the understanding of helium transport: (1) the competition between self-interstitials and helium atoms to react with vacancies; (2) helium atoms tend to agglomerate with radiation-induced and thermal vacancies; (3) displacement collision cascades can supply enough energy to remove helium "bound" to vacancies or HeVCs. To model helium transport in the bulk material during irradiation, in addition to the above processes, various possible helium diffusion mechanisms must also be taken into account. Thus the diffusion of helium through bulk material during irradiation is influenced by the following processes:

1) Trapping and de-trapping of helium in single vacancies, di-vacancies, and higher order clusters;

2) Helium trapping at dislocations and grain boundaries;

3) Replacement of helium bound to single vacancies by self-interstitials;

4) Helium clustering into h-v complexes;

5) Displacement of trapped helium atoms by irradiation;

6) Migration of helium as an interstitial atom or in a highly mobile di-vacancy.

Ignoring the majority of the above possibilities, simplified models for helium diffusion in irradiated materials have previously been developed.[8-12] In this study, all of the reactions outlined above are included. This is accomplished by using chemical rate theory to describe clustering events between randomly migrating species. This method has been used previously to calculate nucleation rates of fission gas bubbles in nuclear fuels.[13] More recently Russell and Hall[14] used chemical reaction rate theory to analyze point-defect clustering in the presence of mobile helium atoms. We developed a model[6] which accounts for the mutual interactions of clustering and migration processes of helium atoms under irradiation. This is the main difference between our approach and previous attempts.[9-12]

With the basic assumption that helium point-defect interactions are homogenous in time and space, a detailed set of rate equations was solved both analytically and numerically.[6] Analytical expressions for the effective diffusion coefficient of helium were derived. Diffusion regimes in the parameter space of displacement damage rate, temperature, helium generation rate, and sink strength were defined. For metals such as steels and nickel, the effective helium diffusion coefficient is dictated by three different physical processes: radiation displacement at low temperatures ($T < 400$ K), self-interstitial replacement at intermediate temperatures ($400 < T < 800$ K), and thermal de-trapping at high temperatures ($T > 800$ K). Our

helium transport model developed earlier[6,7] is used here for the phase-space analysis of nucleation and evolution as outlined below.

3 PHASE-SPACE ANALYSIS OF NUCLEATION AND EVOLUTION

In general, atomic clustering processes have to overcome a nucleation energy barrier. If the nucleation barrier is small or negligible, the formation of stable cluster nuclei proceeds spontaneously. In cases of high nucleation energy barriers, the formation of critical or stable clusters is only dictated by a stochastic process in which the stable configuration is achieved through infrequent chance encounters of necessary constituents. The nucleation of cavities in irradiated solids involves the exchange of at least two species (the vacancy and the SIA) between the cluster and the lattice. In the presence of helium, three species must be considered in these nucleation and growth processes. Helium has a strong catalyzing effect on the nucleation of cavities. Helium atoms enter the cavity and help support the surface energy forces through internal pressure.

To include the effects of mobile helium atoms and a continuous source of helium, vacancy, and SIA, a unified treatment of the nucleation process was developed by Russell[15] using the nodal line analysis. The nodal line analysis of HeCVs begins by considering cavities as characterized in a 2-D phase space (Figure 1), where a cluster is characterized by the number of vacancies and the number of helium atoms it contains. In Figure 1, β stands for capture and α for loss reaction frequencies of vacancies (v), SIAs (i), helium atoms (h), and K_h^r represents the helium replacement reaction rate caused by dynamic momentum transfer from primary knock-on atoms (PKAs).

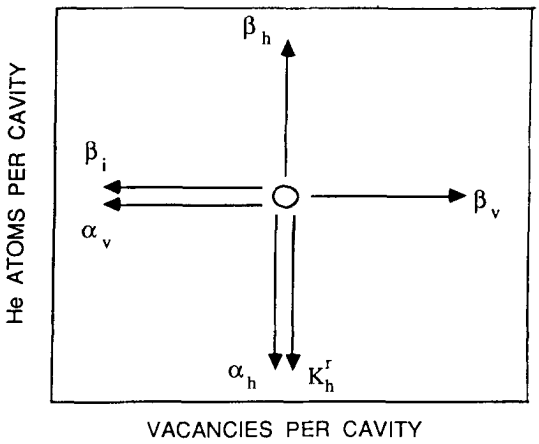

FIGURE 1 Phase space for cavity nucleation showing movements of a cavity following possible point-defect capture (β_v, β_i, β_h) or loss (α_v, α_h, K_h^r).

The behavior of a cluster containing a number of vacancies and helium atoms in this phase space can be characterized by phase-space velocities which equal the sums of jump frequencies times the respective unit jump vector (neglecting higher mobile defects such as di-vacancies):

$$\frac{dv}{dt} = R_v^c - R_v^e - R_i^c, \tag{1}$$

$$\frac{dh}{dt} = R_h^c - R_h^e - R_i^{gr} - R_h^r, \tag{2}$$

where, R_v^c is the single-vacancy capture rate, R_h^c the helium-atom capture rate, R_v^e the vacancy emission rate, R_i^c the SIA capture rate, R_h^e the helium-atom emission rate, R_i^{gr} the gas replacement rate caused by interaction with an SIA, and R_h^r is the helium re-solution rate caused by PKAs. In the present work, these reaction rates are calculated using (1) atomistic binding energy results[16]; (2) binding energies based on high-density EOS for helium[5]; and (3) quasi-steady-state values for the vacancy, helium atoms, and SIA concentrations in the bulk material. Details of these calculations can be found in Ref. 7.

Setting dv/dt and dh/dt equal to zero and plotting the loci of these points in the h-v phase space, helium and vacancy nodal lines are established. A possible configuration of nodal lines is schematically shown in Figure 2.

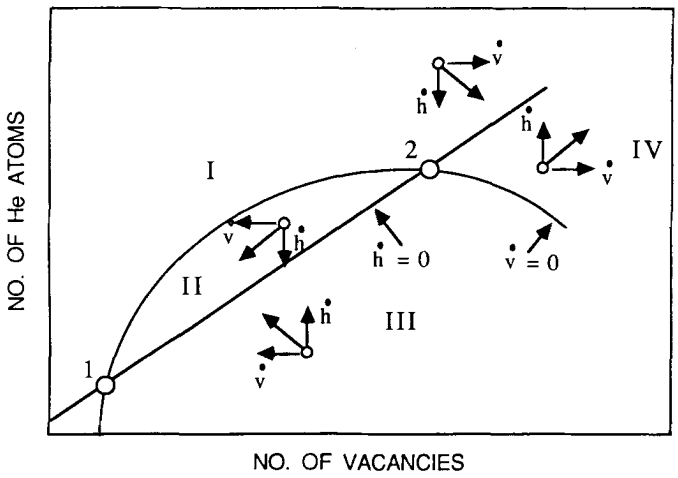

FIGURE 2 Schematic of possible nodal lines showing regions of growth and shrinkage of HeVCs in an h-v phase space.

It can be observed from the figure that:

- In region I, HeCVs grow by vacancy addition but shrink by loss of helium atoms.
- In region II, HeCVs shrink by loss of both vacancies and helium atoms.
- In region III, HeVCs grow by helium addition but shrink by loss of vacancies.
- In region IV, HeCVs grow by addition of both vacancies and helium atoms.

The two points marked 1 and 2 on the phase diagram are determined by simultaneously setting $\dot{v} = \dot{h} = 0$. In region IV, HeVCs will grow unstably to larger sizes, as long as the helium and vacancy supply continues.

Using the nodal line analysis method, two nucleation modes are determined. The first mode causes a spontaneous helium precipitation into cavities (see Figure 3). Very small nucleation barriers exist in this case and nucleation proceeds homogeneously in the matrix. This occurs under the following irradiation conditions: high helium-generation rates, low temperatures, and low sink densities. The high helium-generation rate tips the competition for vacancies between SIAs and helium atoms in favor of helium atoms. This reduces vacancy annihilation rates due to SIAs, and thus the chance for survival of fundamental HeVCs is enhanced.

In the second mode, which is termed stochastic nucleation, cavity formation proceeds with substantial nucleation barriers (i.e., regions I, II, or III in Figure 3), which must be overcome by stochastic size fluctuations of subcritical HeVC embryos in order to reach stable configurations. This case is best achieved at high temperatures, low dislocation sink densities, and low helium-generation rates. The combination of high temperature and high sink density results in short defect mean-life times. These, coupled with low helium-generation rates, increase the

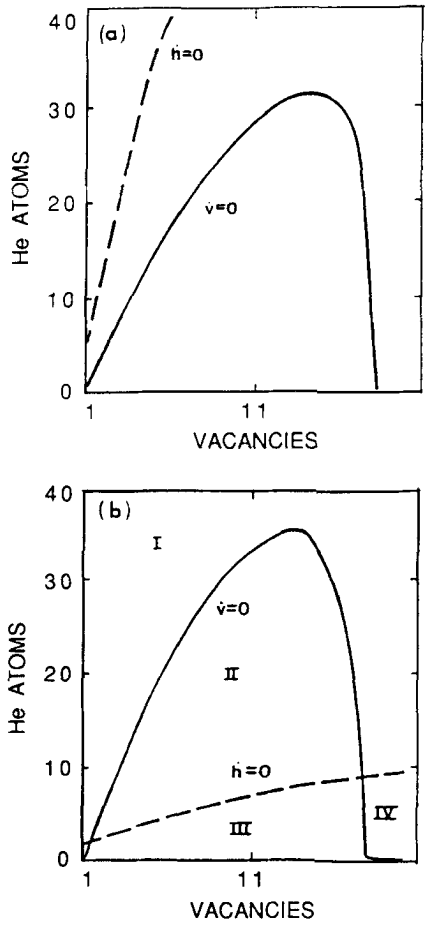

FIGURE 3 Stability analysis for HeVCs showing nucleation ($T = 500°C$, displacement damage rate $= 10^{-6}$ dpa/s, dislocation density $= \rho_d = 10^{10}$ cm^{-2}): (a) Spontaneous (He/dpa = 57); (b) Stochastic (He/dpa = 0.1).

chances of SIAs to compete successfully against helium atoms for vacancies. These effects (nucleation barriers) suppress the generation of stable HeCV embryos. Therefore, to overcome the nucleation barrier, stable HeVCs must be formed by a stochastic process.

A parametric study of various irradiation conditions and material properties at different temperatures was performed.[7] For typical fusion and ion implantation environments it was shown that nucleation of stable HeVCs will be spontaneous. In this work we deal only with the spontaneous nucleation and growth of HeCVs.

4 CLUSTERING MODEL AND THE FOKKER-PLANCK EQUATION

Ghoniem *et al.*[6,7] formulated a detailed rate theory for the transport and early clustering of h-v complexes. It has been shown that transport and clustering cannot be easily separated, at least not during the transient phase of nucleation. However, under conditions of high He/dpa ratios, a cluster containing only three helium atoms may be an adequate critical size. An important consequence of this mode of nucleation is that nucleation proceeds on a relatively fast time scale compared to growth or evolution time scales. When nucleation is completely stochastic, as in the case of very low concentration of gas atoms, temporal separation between nucleation and growth is not possible. In this section, we follow the general outline of the theory developed by Ghoniem *et al.*[6,7] Furthermore, we use the fact that the nucleation time scale is several orders of magnitude smaller than the evolution time scale at high He/dpa ratios.

The nucleation rate of critical size HeCVs is given by

$$\frac{dC^*}{dt} = R_{g,2gv} C_g C_{2gv} + R_{g2g} C_g C_{2g} - R_{g,*} C_g C^* - R_{v,*} C_v C^* - R_{i,*} C_i C_* - 3bGC^*. \quad (3)$$

Here $R_{A,B}$ represents the reaction rate between A and B type clusters. The subscript/superscript notation is as follows: g = gas; v = vacancy, i = interstitial, and * = all h-v cavities containing three or more gas atoms. The displacement rate is denoted by $G(s^{-1})$, and the probability of gas re-solution into the matrix by b (per gas atom). The reaction rates are for single-step atomic transitions and represent mean values of successful atomic transition probabilities. The concentration of critical size nuclei (C^*) is naturally dependent upon the concentrations of various HeVCs, as well as on the concentration of single-helium interstitials and SIAs. This information is obtained from the complete model developed by us earlier.[6,7] and therefore will not be repeated here. The point of departure here is that the total cavity density is determined, as a function of time from Eq. (3), and is then used in the F-P calculations as will be discussed below.

We first define the following: v = number of vacancies in a cluster, h = number of helium atoms in a cluster, and $P(v, h, t)dvdh$ = probability of a cluster at time t in the interval $(v, v+dv)$ and $(h, h+dh)$. The concentration of clusters containing v vacancies and h helium atoms at time t is approximately given by $C(v, h, t) = C^*(t)P(v, h, t)$. The time evolution of the probability function in terms

of all possible transitions in the h-v phase space is given by the master equation (ME):[17]

$$\frac{dP(h, v, t)}{dt} = \sum_{\theta} w\{[(v-\Delta v_\theta), \quad (h-\Delta h_\theta)] \rightarrow (v, h)\} \times P[(v-\Delta v_\theta), \quad (h-\Delta h_\theta), t] - \sum_{\theta} w\{(v, h) \rightarrow [(v+\Delta v_\theta), \quad (h+\Delta h_\theta)]\} P(v, h, t). \tag{4}$$

Here Δv_θ is a fluctuation in the vacancy content caused by a stochastic process θ, and Δh_θ is a similar fluctuation in the helium content: transition probabilities for the various processes are w and their statistical properties can be obtained from the detailed physics of the process. The ME form given by Eq. (4) is based upon the Smolochoiski–Chapman–Kolmogorov (SCK) equation,[17] and the atomic transitions in Eq. (4) represent Gaussian–Markovian processes. Following Nicolis and Prigogine,[17] we multiply Eq. (4) by an arbitrary smooth function $Q(v, h)$, which goes with sufficient rapidity to zero as $(v, h) \rightarrow \infty$. Integrating the resulting equation over the h-v space and expanding $Q(v, h)$ around $Q(v-\Delta v_\theta, h-\Delta h_\theta)$ and switching to new integration variable $v' = v - \Delta v_\theta$ and $h' = h - \Delta h_\theta$, we obtain, up to second order, the Kramers-Moyal expansion to the h-v clustering equation [Eq. (4)]:

$$\iint Q(v, h) \frac{\partial P}{\partial t} dv\, dh = \sum_{\theta} \iint \Bigg\{ w[(v, h) \rightarrow (v+\Delta v_\theta, h)] \Delta v_\theta \frac{\partial Q}{\partial v} + w[(v, h) \rightarrow (v, h+\Delta h_\theta)] \Delta h_\theta \frac{\partial Q}{\partial h} \Bigg\} + \frac{1}{2!} \Bigg\{ w[(v, h) \rightarrow (v+\Delta v_\theta, h)] \Delta v_\theta^2 \frac{\partial^2 Q}{\partial v^2} + w[(v, h) \rightarrow (v, h+dh_\theta)] \Delta h_\theta^2 \frac{\partial^2 Q}{\partial h^2} + 2w[(v, h) \rightarrow (v+\Delta v_\theta, h+\Delta h_\theta)] \times \Delta v_\theta \Delta h_\theta \frac{\partial^2 Q}{\partial v\, \partial h} \Bigg\} P\, dv\, dh. \tag{5}$$

The subscript θ is used to indicate the *type* of the independent stochastic process. We can consider three types of transitions: (1) those caused by a single vacancy or a single-helium atom, (2) multiple vacancy transitions resulting from diffusion out of a nearby cascade, and (3) multiple h-v transitions caused by direct collisions between cascade recoils and the contents of a cavity. For the first mechanism we use the subscript $\theta = s$, for the second $\theta = cd$, and for the third $\theta = cc$. In developing Eq. (5) we neglect terms containing $O(\Delta v_\theta^3, \Delta h_\theta^3)$. For a Gaussian–Markovian stochastic process, moments beyond the second for the transition probabilities $w(v, h)$ vanish.

Now the first and second moments of the transition probability are given by

$$a_{1v} = w[(v, h) \rightarrow (v + \Delta v_s, h)]\Delta v_s + w[(v, h) \rightarrow (v + \Delta v_{cd}, h)]\Delta v_{cd} + w[(v, h) \rightarrow (v + \Delta v_{cc}, h)]\Delta v_{cc}; \tag{6}$$

$$a_{1h} = w[(v, h) \rightarrow (v, h + \Delta h_s)]\Delta h_s + w[(v, h) \rightarrow (v, h + \Delta h_{cc})]\Delta h_{cc}; \tag{7}$$

$$a_{2vv} = \frac{1}{2!}\left\{ w[(v, h) \rightarrow (v + \Delta v_s, h)](\Delta v_s)^2 + w[(v, h) \rightarrow (v + \Delta v_{cd}, h)](\Delta v_{cd})^2 + w[(v, h) \rightarrow (v + \Delta v_{cc}, h)](\Delta v_{cc})^2 \right\}; \tag{8}$$

$$a_{2hh} = \frac{1}{2!}\left\{ w[(v, h) \rightarrow (v, h + \Delta h_s)](\Delta h_s)^2 + w[(v, h) \rightarrow (v, h + \Delta h_{cc})](\Delta h_{cc})^2 \right\}; \tag{9}$$

$$a_{2vh} = w[(v, h) \rightarrow (v + \Delta v_s, h + \Delta h_s)](\Delta v_s \Delta h_s) + w[(v, h) \rightarrow (v + \Delta v_{cc}, h + \Delta h_{cc})](\Delta v_{cc} \Delta h_{cc}). \tag{10}$$

The moments given by Eqs. (6)–(10) can be evaluated if we assume that the process is ergodic, and hence the ensemble averages are equal to temporal averages over a suitable correlation time. Later in this section, we will discuss how the moments can be evaluated for single-step atomic transition processes.

Equation (5) now becomes:

$$\iint Q \frac{\partial P}{\partial t}\, dv\, dh = \iint P\left(a_{1v}\frac{\partial Q}{\partial v} + a_{1h}\frac{\partial Q}{\partial h} + a_{2vv}\frac{\partial^2 Q}{\partial v^2} + a_{2hh}\frac{\partial^2 Q}{\partial h^2} + a_{2vh}\frac{\partial^2 Q}{\partial v\, \partial h} \right) dv\, dh. \tag{11}$$

Following the methods of non-equilibrium statistical mechanics,[18] we integrate Eq. (11) by parts in the right-hand side and use the fact that Q is an arbitrary function to obtain the following F-P equation:

$$\frac{\partial P}{\partial t} = -\left[\frac{\partial}{\partial v}(a_{1v}P) + \frac{\partial}{\partial h}(a_{1h}P) \right] + \left[\frac{\partial^2}{\partial v^2}(a_{2vv}P) + \frac{\partial^2}{\partial h^2}(a_{2hh}P) + \frac{\partial^2}{\partial v\, \partial h}(a_{2vh}P) \right]. \tag{12}$$

Figure 1 shows possible single-atom transitions in the h-v phase space. In this schematic, the effects of cascades on the transition moments will be neglected. In this 2-D phase space, we define a drift vector, $\mathbf{F}(v, h)$, and a diffusion tensor, $\boldsymbol{D}(v, h)$, as follows:

$$\mathbf{F}=\begin{bmatrix} a_{1v} \\ a_{1h} \end{bmatrix},$$

$$\boldsymbol{D}=\begin{bmatrix} a_{2vv} & a_{2vh} \\ a_{2hv} & a_{2hh} \end{bmatrix}.$$

It is worthwhile to cast Eq. (12) in the familiar continuity form by using a simple definition of the probability density current as:

$$\mathbf{J}=\mathbf{F}P-\nabla(\boldsymbol{D}P). \tag{13}$$

The probability evolution equation [Eq. (12)] can now be compactly stated as:

$$\frac{\partial P}{\partial t}+\nabla\cdot\mathbf{J}=0. \tag{14}$$

A numerical solution to Eq. (14) will be presented in the next section.

Before we proceed, however, we describe a method for evaluating the components of the vector $\mathbf{F}$ and the tensor $\boldsymbol{D}$ when cascade effects are neglected, as shown in Figure 1. Here we use the notation K^{xy} for the rate constant of process xy. We consider here the following atomic transition processes:

ic = self-interstitial capture,
vc = vacancy capture,
gc = helium atom capture,
gr = helium atom replacement,
ge = helium atomic thermal emission,
ve = vacancy thermal emission.

In the case of single-step atomic transitions treated here, the jumps $(\Delta v, \Delta h)$ are either ± 1 as shown in Figure 1. Now applying Eqs. (6)–(10), we obtain:

$$a_{1v}=k^{vc}-(k^{ic+vc}+k^{gr}), \tag{15}$$

$$a_{1h}=k^{gc}-(k^{ge}+k^{gr}), \tag{16}$$

$$a_{2vv}=\frac{1}{2!}(k^{ic+vc}+k^{gr}+k^{vc}), \tag{17}$$

$$a_{2hh}=\frac{1}{2!}(k^{gc}+k^{gr}+k^{gc}), \tag{18}$$

$$a_{2vh}=a_{2hv}=k^{gr}. \tag{19}$$

The values of the transition moments given by Eqs. (15)–(19) are evaluated from the solution of a coupled set of rate equations developed by Ghoniem *et al.*[6, 7] The implications of fluctuations with $(\Delta v, \Delta h) \gg \pm 1$ caused by cascades will be discussed later when we present our numerical results.

5 NUMERICAL ANALYSIS OF THE FOKKER-PLANCK EQUATION

Finite differencing the F-P equation, Eq. (14), transforms the partial differential equation into a set of ordinary differential equations (ODEs). One of the major characteristics of these ODEs is their stiffness which stems from the large differences in the reaction rate constants (transition probabilities) between clusters of different sizes. Small clusters transform rapidly into larger ones and, with this increase in size, transformations slow down. The stiffness of the system is particularly severe in this study because the current model encompasses HeVCs containing between 3 and 10^7 defects. This stiffness is further compounded by vastly differing reaction rates for helium and vacancies.

In this work, we use the latest version of the LSODE package,[19] which was developed for initial value problems of stiff and non-stiff systems of first order ODEs. The user has the option to use either implicit Adams methods or a variety of explicit integration schemes. We found that the backward differentiation method with a mean-chord iteration and the numerical generation of the full Jacobian as the most suitable option for our system of equations. An important feature of this ODE solver is the ability to stop the numerical integration at any desired time and to re-start as a new initial-value problem with modified initial conditions. This enables the user to examine the progress of the solution. Furthermore, it re-initializes internal solver step sizes allowing the user to add or delete equations from the system of equations being solved. This feature of the LSODE package is particularly useful for developing a dynamic re-meshing algorithm as described later in this section.

The current **J** in Eq. (14) consists of two components:

$$\mathbf{J} = \mathbf{e}_h J^h + \mathbf{e}_v J^v, \tag{20}$$

where $\mathbf{e}_{h,v}$ are unit vectors in helium and vacancy direction in a h-v phase space, respectively; and J^h is given by

$$J^h \equiv [J(h, t)]_v = \left\{ F^h C(h, t) - \frac{\partial}{\partial h} [D^h C(h, t)] \right\}_v, \tag{21}$$

and the vacancy current J^v

$$J^v \equiv [J(v, t)]_h = \left\{ F^v C(h, t) - \frac{\partial}{\partial v} [D^v C(h, t)] \right\}_h. \tag{22}$$

In short form notation, Eqs. (21) and (22) can be written as:

$$J^h = [F^h C]_v - \left[\frac{\partial}{\partial h} D_h \mathrm{C} \right]_v, \tag{23}$$

$$J^v = [F^v C]_h - \left[\frac{\partial}{\partial v} D^v C \right]_h. \tag{24}$$

Considering a conservative phase element $(\Delta v, \Delta h)$, and integrating Eq. (14) at an (i, j) meshpoint (see Figure 4), we obtain:

$$\int_{h_{i,j-1/2}}^{h_{i,j+1/2}} \int_{v_{i-1/2,j}}^{v_{i+1/2,j}} \partial v \, \partial h \, \frac{\partial P_{i,j}}{\partial t}$$

$$= -\int_{h_{i,j-1/2}}^{h_{i,j+1/2}} \int_{v_{i-1/2,j}}^{v_{i+1/2,j}} \partial v \, \partial h \left(\frac{\partial J_{i,j}}{\partial h} + \frac{\partial J_{i,j}}{\partial v} \right). \tag{25}$$

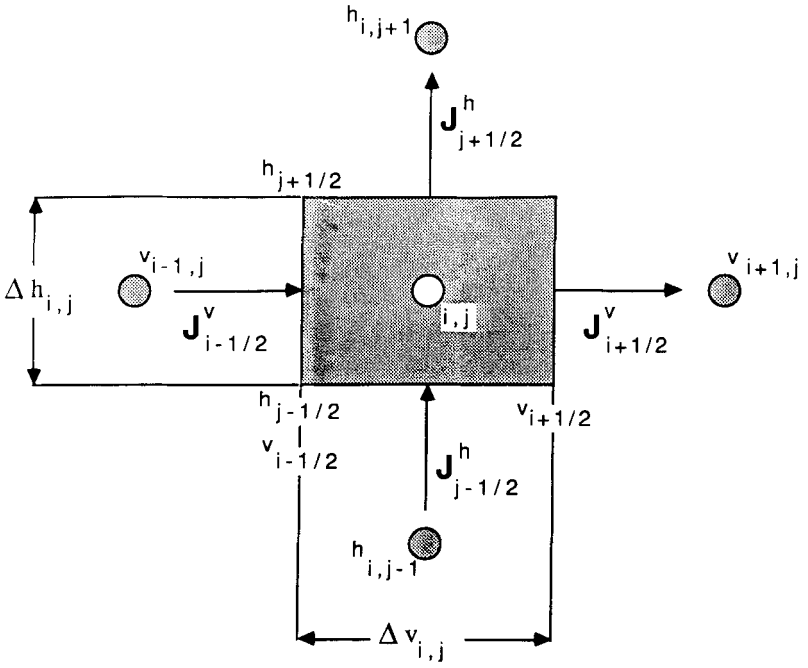

FIGURE 4 Notations and coordinates of the i, j-th element in an h-v phase space.

Using central differencing, we get for the vacancy directions the following mesh spacing:

$$[\Delta v_i]_j = [v_{i+1/2} - v_{i-1/2}]_j, \tag{26}$$

and

$$[v_{i+1/2}]_j \equiv \left[\frac{1}{2} (v_{i+1} + v_i) \right]_j, \tag{27}$$

$$[v_{i-1/2}]_j \equiv \left[\frac{1}{2} (v_i + v_{i-1}) \right]_j. \tag{28}$$

Combining Eqs. (26)–(28) we get:

$$[\Delta v_i]_j \equiv \left[\frac{1}{2}(v_{i+2} - v_{i-1})\right]_j . \tag{29}$$

Similarly in the helium direction, for the mesh size dimension we get:

$$[\Delta h_i]_j \equiv \left[\frac{1}{2}(h_{j+2} - h_{j-1})\right]_i . \tag{30}$$

Using finite differences, Eq. (25) is now represented by a finite number of discrete equations of the form:

$$\frac{\partial P_{i,j}}{\partial t} = \frac{1}{[\Delta h_j]_i}\left[J^h_{low} - J^h_{upp}\right]_i + \frac{1}{[\Delta v_i]_j}\left[J^v_{low} - J^v_{upp}\right]_j , \tag{31}$$

where J^h_{low}, J^h_{upp}, J^v_{low}, and J^v_{upp} are given by Eqs. (23) and (24) finite differenced at $[i, j-(1/2)]$, $[i, j+(1/2)]$, $[i-(1/2), j]$, and $[i+(1/2, j]$, respectively.

An advantage of Eq. (31) is the convenience with which the conservation principle can be implemented, provided a finite solution space is established. The following section outlines a trajectory method approach to construct a finite solution space for our system of ODEs.

5.1 *The Trajectory Method for Determining Average Cavity Sizes*

Trinkaus[20] used an analytical formulation to predict the average h-v ratio in the h-v phase space for constant single-helium atom and vacancy fluxes. This approach is used and expanded to include time-dependent helium and vacancy fluxes.

We start with the growth equation of clusters via vacancy absorption, which is expressed as the difference between single vacancy and SIA impingement fluxes:

$$\frac{dR}{dt} = \frac{1}{R}\left(D_v C_v - D_i C_i - D_v C_v^e\left\{\exp\left[\frac{\Omega}{kT}\left(\frac{2\gamma}{R} - p\right)\right] - 1\right\}\right), \tag{32}$$

where $D_v C_v$, $D_i C_i$, and $D_v C^e$ are single vacancy, interstitial, and thermal vacancy fluxes, respectively. R is the cluster radius, Ω the atomic volume, and k is the Boltzmann's constant. The last term in Eq. (32) represents the vacancy emission rate which is a function of the pressure p, the surface tension of the cavity γ, and the temperature T.

In the analytical work of Trinkaus,[20] the assumption is made that helium atoms do not return to the matrix once captured. Thus the helium growth equation is the capture rate of helium atoms given by the helium growth equation

$$\frac{dh}{dt} = \frac{4\pi R}{\Omega} D_{He} C_{He} . \tag{33}$$

Equation (33) depends on the helium flux $D_{He}C_{He}$, which itself depends on the cavity concentration C_B. This poses a problem for analytical solutions. Therefore, the helium growth equation [Eq. (33)] was simplified by assuming that all helium produced is distributed equally among all the cavities:

$$\frac{dh}{dt} = \frac{P_{He}}{C_B \Omega}, \tag{34}$$

where p_{He} is the helium generation rate. Equation (34) also assumes no loss of helium to other sinks such as grain boundaries and precipitates. In the present work these assumptions are removed and furthermore we include a re-solution term in the helium growth equation:

$$\frac{dh}{dt} = \frac{4\pi R}{\Omega}(D_{He} C_{He}) - Nb, \tag{35}$$

where b is the probability of re-solution per helium atom per unit time, and N is the number of helium atoms per HeVC. Because we are solving a detailed set of rate equations, the vacancy growth equation [Eq. (32)] is expressed in terms of v, the number of vacancies per HeVC:

$$\frac{dv}{dt} = \frac{4\pi R}{\Omega}\left(D_v C_v - D_i C_i - D_v C_v^e\left\{\exp\left[\frac{\Omega}{kT}\left(\frac{2\gamma}{R} - p\right)\right] - 1\right\}\right). \tag{36}$$

In this work, the gas pressure, p, is given by Van der Waal's EOS:

$$p = \frac{NkT}{(4/3)\pi R^3 - NB}, \tag{37}$$

where B is Van der Waal's constant. For high gas pressures and small radii, a virial expansion is used for greater accuracy:

$$p = \frac{NkT}{v\Omega}\left[1 + \left(\frac{NB}{v\Omega}\right) + \left(\frac{NB}{v\Omega}\right)^2 + \left(\frac{NB}{v\Omega}\right)^3 + \left(\frac{NB}{v\Omega}\right)^4 + \ldots\right], \tag{38}$$

where $v\Omega$ is the volume occupied by v vacancies.

The growth trajectory is determined using Eqs. (35) and (36) by numerically integrating:

$$\frac{dv}{dh} = f(v, h), \tag{39}$$

where the function $f(v, h)$ is the ratio of the right-hand sides of Eqs. (35) and (36). Thus the trajectory depends on the three basic defect fluxes (v, i, h) and a helium re-solution parameter (b).

Examples of the numerical solution of Eq. (39) are shown in Figure 5 for various irradiation facilities. HFIR and EBR-II have similar displacement damage rates of $\sim 10^{-6}$ dpa/s but differ in the helium generation rate. Accelerators generally deliver a displacement rate on the order of $\sim 10^{-3}$ dpa/s with high He/dpa ratios of ~ 100 appm/dpa. Figure 5 shows the effects of He/dpa ratios on the helium content of cavities.

The effects of the ideal gas law and thermodynamic equilibrium on the trajectories are examined in Figure 6. Thermodynamic equilibrium assumes that the pressure is in equilibrium with the surface tension force of the cavity. We also compare the trajectory for EBR-II irradiation conditions using Van der Waal's EOS

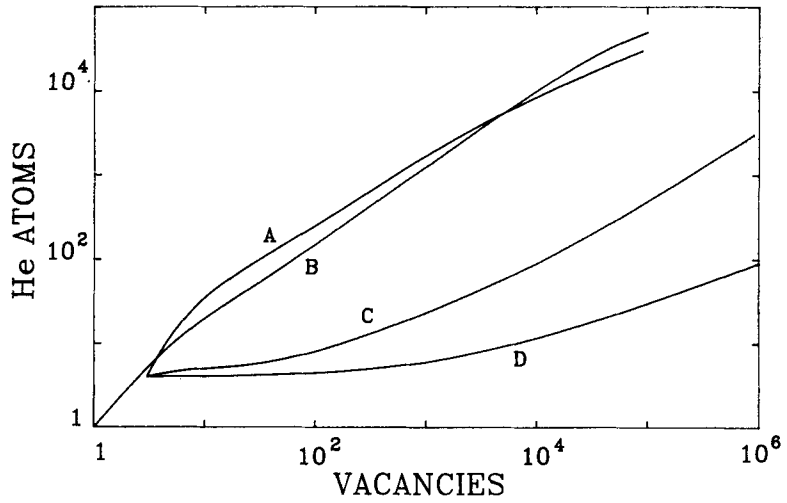

FIGURE 5 Growth trajectories for accelerator (A), HFIR (C), and EBR-II (D) irradiation conditions at 500°C (B = equilibrium bubbles).

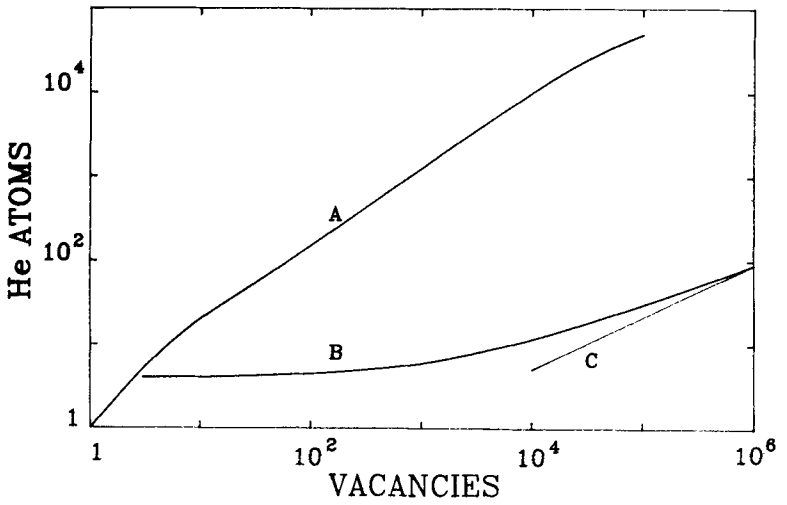

FIGURE 6 Growth trajectories for EBR-II irradiation conditions at 500°C using Van der Waal's EOS (B) and the ideal gas law (C) to describe the pressure inside HeVCs (A = equilibrium bubbles).

and the ideal gas law. As the size of HeVcs increases, the ideal gas law trajectory approaches that of the Van der Waal EOS trajectory.

The effects of the re-solution parameter are shown in Figure 7. Even though the effect of re-solution is negligible on small HeVCs containing less than 10^4 vacancies, it becomes an important parameter in determining the helium content of larger cavities.

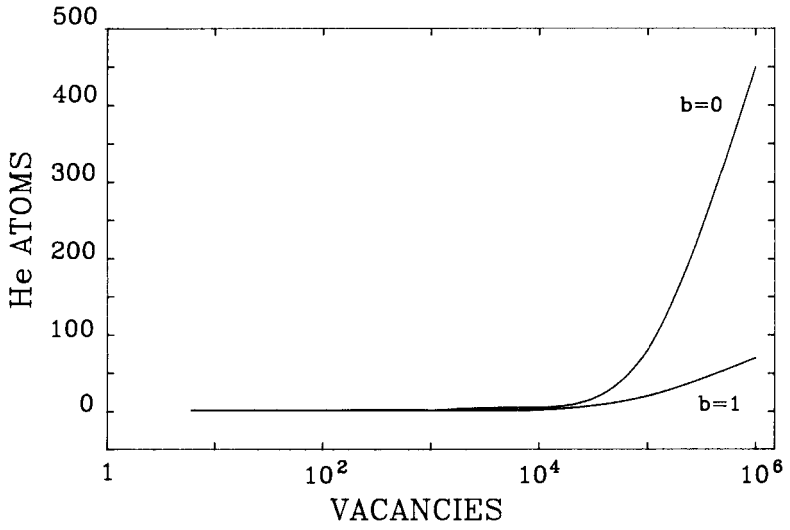

FIGURE 7 Effect of re-solution parameter (b) on the growth trajectories for EBR-II irradiation conditions using Van der Waal's EOS and the ideal gas law to describe the pressure inside HeVCs.

5.2 *Solution Space for the Fokker–Planck Equation*

The growth trajectory of HeVCs in the h-v phase space gives the average size of HeVCs. To develop a numerical solution of the F-P equation we need to determine a finite solution space around the trajectory. The approach is to conserve the zero-th moment of the probability distribution function by invoking zero-current boundary conditions on a prescribed contour in the h-v phase space. This contour should conserve, at all times, the zero-th moment of the distribution function. It is therefore necessary to define the zero-current contour around the trajectory. The extent of the chosen solution space should be determined by higher moments of the distribution function. A reasonable choice is based on the second moment, which is described below.

Starting with growth equations $\dot{v}$ and $\dot{h}$ [Eqs. (35) and (36)], we can quantify a diffusional spread in the vacancy and helium directions as follows:

$$\langle \Delta v \rangle^2 \equiv 4D^v \tau, \tag{40}$$

$$\langle \Delta h \rangle^2 \equiv 4D^h \tau, \tag{41}$$

where D^v and D^h are determined from the corresponding growth equations:

$$D^v = \frac{2\pi R}{\Omega}\left(D_v C_v + D_i C_i + D_v C_v^e\left\{\exp\left[\frac{\Omega}{kT}\left(\frac{2\gamma}{R} - p\right)\right] - 1\right\}\right), \tag{42}$$

$$D^h = \frac{2\pi R}{\Omega}(D_{\mathrm{He}} C_{\mathrm{He}}) + \frac{1}{2} Nb. \tag{43}$$

A numerical approach must be used to calculate the time τ, corresponding to every h-v combination on the trajectory. This can be evaluated from:

$$\tau = \int_{v^*}^{V} \frac{dv'}{f(v', h)} = \int_{h^*}^{H} \frac{dh'}{f(v, h')}, \tag{44}$$

where the integration is a line integral along the trajectory from either v^* or h^* to V or H.

As a conservative estimate for the diffusional spread in the h-v size space, we used a multiple of the estimates given by Eq. (40) and (41). A factor between 5 and 10 is found to be reasonable. Figure 8 shows the results of sample calculations, where the contours are obtained with five times the average spreads given by Eqs. (40) and (41). Note that the diffusional spreads of helium and vacancies trace different loci. This is because of the differences in diffusion rates. As a rule, we chose the larger of the two spreads. In case of HFIR irradiation conditions, the boundaries are determined by the helium diffusional spreads (see Figure 8). Therefore the loci determined by the diffusional spreads around the trajectory constitute the boundaries of the solution space across which no cavity evolution current flows. Thus we have constructed a finite, closed boundary system, provided we establish a maximum possible HeVC size.

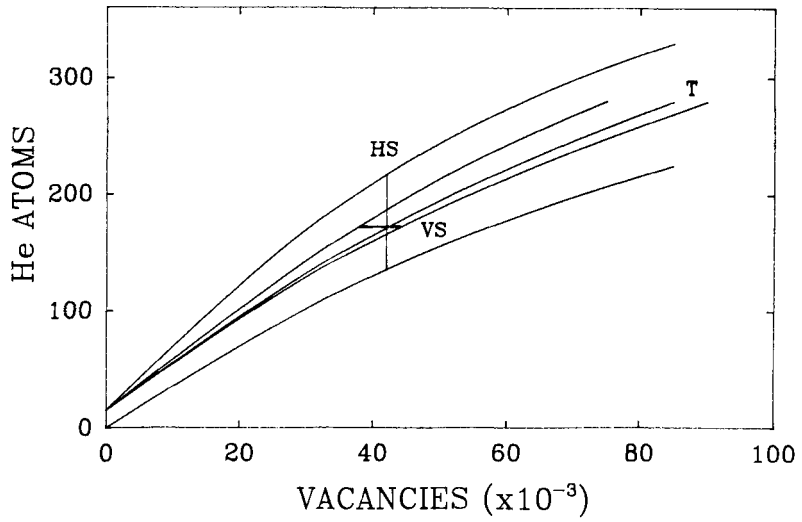

FIGURE 8 Growth trajectories (T) for HFIR irradiation conditions at 500°C using Van der Waal's EOS showing estimated diffusional spreads in the helium (HS) and vacancy (VS) directions.

5.3 *Boundary Conditions*

A set of detailed rate equations is solved for small clusters resulting in a self-interstitial flux, a helium-atom flux, a single-vacancy flux, and a critical HeVC nucleation current. Once quasi-steady-state flux rates are reached, mobile defect fluxes and the concentration of critical HeVCs are taken as input parameters to the F-P equations. This separation of nucleation and growth is reasonable, since nucleation time scales are much shorter than growth time scales in this particular situation.

Temporal separation between nucleation and growth, together with application of Gauss's divergence theorem on Eq. (14), results in $\oint \mathbf{J} \cdot \mathbf{dl} = 0$ around the solution space boundary. If at the upper boundary the current leaving the solution space (J_{out}) is zero, the total number of HeVCs is conserved at all times. This conservation principle thus constitutes a check on the numerical solution to the F-P equation. As a case study, we consider the HFIR irradiation conditions and stainless-steel material parameters. Figure 9 shows the behavior of the HeVC size distribution at different irradiation times without helium in order to ascertain the numerical accuracy of the method. At the onset of the evolution ($t_1 = 0.1$ s), the distribution is shown to be dominated by small clusters. At $t_2 = 8.6 \times 10^3$ s, we notice a decrease in the concentration of critical HeVCs and a broadening of the distribution. Because the nucleation current (J_{in}) is set equal to zero, there is no supply of critical HeVCs. As irradiation continues, the distribution function broadens and the peak amplitude decreases.

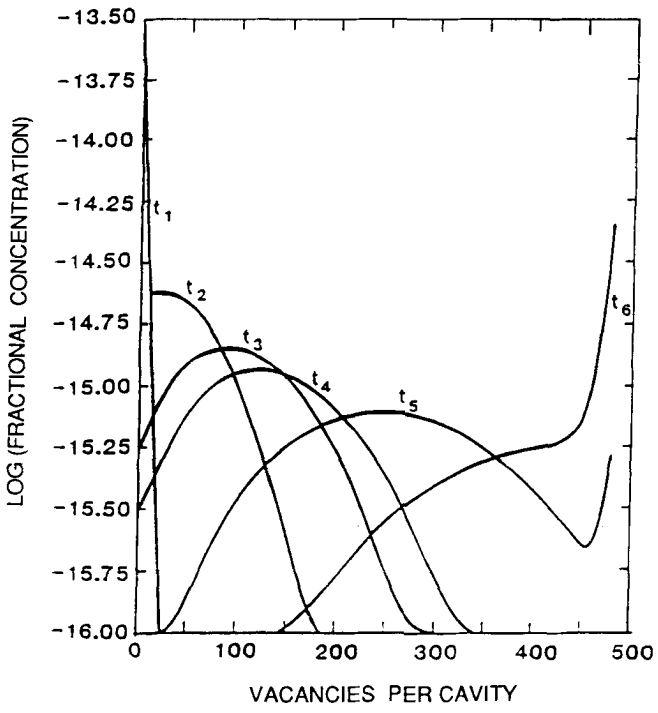

FIGURE 9 The evolution of small HeVCs using the F-P equation and the zero-current boundary condition for typical HFIR irradiation conditions.

This behavior is expected from a F-P equation in which the drift term F forces the peak to move while the diffusion term D causes a broadening around the peak. Because we have set J_{out} equal to zero, there are no destruction mechanisms for the largest HeVCs. The calculations indicate that the number density of large clusters increases steadily at the expense of smaller ones. Thus, once the peak has reached the maximum size considered, it stays at that position and its value steadily increases until about 10^5 s of irradiation time. Beyond this time, the distribution

remains unchanged for any practical irradiation time considered. The conservation of the zero-th moment of the HeVC distribution was checked using a simple trapezoidal integration rule. The largest error found was on the order of the machine round-off error ($\sim 10^{-14}$ % for the CRAY-1 supercomputer).

The zero-current boundary condition was extended to the helium dimension of the solution space and thus an accurate balance of the total number of vacancies and helium atoms introduced into the system during growth was achieved.

5.4 *Dynamic Re-Meshing of the Solution Space*

The major way to save computer time is to minimize the number of ODEs without sacrificing numerical accuracy. In this section a dynamic re-meshing method which effectively keeps the number of equations to a minimum is outlined.

At the onset of evolution, changes in the distribution function are very rapid. The distribution broadens while the peak moves rapidly to larger sizes. As the distribution moves, its rate of change slows down. Therefore, it is crucial to follow both fast and slow modes in the distribution function. This can be achieved by choosing a fine mesh size for small clusters and increasingly larger mesh sizes for larger ones. The computational algorithm is structured such that, once the peak of the HeVC size distribution function moves to larger sizes, equations describing small sizes are removed from the system and other equations are added to cover the evolution of large HeVCs.

Equations are thus dynamically added to the distribution wavefront as it moves towards larger cluster sizes. Concurrently with the addition of equations to the wavefront, the mesh sizes of the new equations are made larger in both dimensions (the vacancy and the helium atom content). The dynamic solution space changes are made possible only because the trajectory method enables us to approximate the average HeVC sizes. Knowledge of the average cluster sizes allows positioning of the distribution peak far from the boundaries of the solution space.

The following is a summary of the dynamic re-meshing algorithm:

1) We first start with a system of equally spaced mesh points spanning a small range from several to 100 vacancies per HeVC. The boundary currents J_{in} and J_{out} are set equal to zero.

2) At chosen output intervals, the average HeVC size is computed using the trajectory method.

3) If the peak position of the distribution becomes too close to the average HeVC size, then a few equations (5 to 10) are added to the wavefront of the system with larger mesh spacings in both the helium content and vacancy dimensions.

4) At each output interval, a check is run on the small-size part of the distribution (wave trailing). The number of equations contributing less than a fraction of a percent ($\sim 0.05\%$) to the zero-th moment are removed from the system. According to the removal or addition of equations, the boundary conditions are also moved along with the system.

Using this technique, a typical run that follows the evolution of helium-filled cavities from a few constituents to over 10^7 uses no more than about 120 equations at any time to cover the total range. The program efficiency is reflected in the small amount of computational time required for typical runs (between 3 and 7 minutes CRAY-1 time).

6 MODEL APPLICATIONS TO IRRADIATED STAINLESS STEEL

Maziasz[21] investigated the sensitivity of microstructural evolution to increased helium content during neutron irradiation. In particular, he used EBR-II- and HFIR-irradiated samples to study cavity evolution. In his experiments, Maziasz found that the low fluence swelling peaks at 425° to 450°C, as cavities grow among a constant background of finely dispersed cavities present between ~9 to ~14 dpa. This results in a bi-modal cavity distribution characteristic only to this temperature range.

Since HFIR irradiation conditions at 450°C have been identified to result in spontaneous nucleation of HeVCs in stainless steels (see Section 3), the present model is applied to this case.

Before cavities can reach the growth stage, we have to establish the quasi-steady-state concentration of critical HeVCs. As outlined in Section 2, this is accomplished by solving a set of detailed rate equations describing the kinetics of interaction between helium and displacement damage. Typical displacement damage rates for HFIR irradiation conditions are 1.11×10^{-6} dpa/s, and the helium generation rate is 6.35×10^{-11} atom/s. The re-solution parameter b has been set equal to 1, and the dislocation bias factor to $Z_i = 1.08$. The remainder of material parameters are the standard values for Type-316 stainless steel given in Table I.

TABLE I
Standard material parameters for type-316 stainless steel

Notation	Parameter	Value	Units	Ref.
a	Lattice parameter	3.63	Å	—
ρ	Dislocation density	3×10^{11}	cm/cm^3	—
E_i^m	SIA migration energy	0.2	eV	22
E_g^m	Single-He interstitial migration energy	0.1	eV	—
E_v^m	Single vacancy migration energy	1.4	eV	22
E_i^f	SIA formation energy	4.08	eV	23
E_v^f	Vacancy formation energy	1.6	eV	22
γ	Surface energy	6.24×10^{14}	eV/cm^2	23
ν_i	Interstitial vibration frequency	5×10^{13}	s^{-1}	24
ν_g	He vibration frequency	5×10^{13}	s^{-1}	25
ν_v	Vacancy vibration frequency	5×10^{12}	s^{-1}	24
B	Van der Waal's constant	1.75×10^{-23}	cm^3	25
b	Re-solution parameter	1	—	—
Z_i	Interstitial bias factor	1.08	—	—
Ω	Atomic volume	1.1958×10^{-23}	cm^3	26

Figure 10 shows the concentration of single vacancies (C_v), SIAs (C_i), single-helium atoms (C_{He}), as well as critical HeVCs. Although the time structure of C_v and C_i is little affected by the presence of helium, the absolute magnitude of the vacancy concentration in this case is less than in a corresponding study[27,28] without the interaction of helium gas. During the early stages of irradiation, helium is generated as interstitial helium atoms, but is soon trapped when vacancies become available. This mechanism keeps the concentration of untrapped helium atoms low. This trapping eventually leads to the formation of cavities from substitutional helium. The cavity concentration has been reported to be approximately 2×10^{-8}

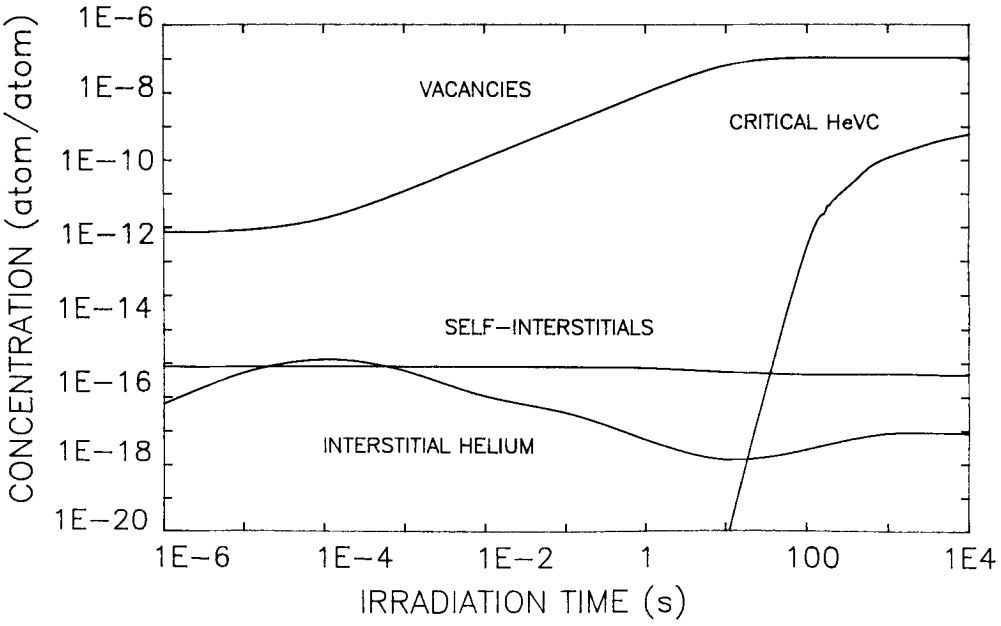

FIGURE 10 Irradiation-produced defects and critical HeVC concentration as a function of irradiation time for HFIR conditions at 450°C.

atom/atom for HFIR irradiation experiments performed at 467°C.[29] Our set of rate equations predicts a critical HeVC concentration of approximately 8×10^{-9} atom/atom (see Figure 10).

Having established the quasi-steady-state concentrations of mobile defects and of critical HeVCs, the trajectory analysis is used to determine the most probable h-v combination of the evolving cavities. Parameters of Table I and the results of the detailed rate equations analysis (Figure 10) are used. The results of the trajectory analysis seem to compare well with the experimental findings of Maziasz[21] (Figure 11). The trajectory analysis also establishes the range of the solution space. Cavities containing up to 10^7 vacancies and 10^5 helium atoms (see Figure 12) were considered in our work. Since the trajectory traces the path of the average h-v combination, we assumed that contributions to the distribution of HeVCs located far from the trajectory are negligible. The outer boundaries were determined using the diffusional spread as outlined in Section 2. Figure 12 shows the solution space around the trajectory containing more than 99% of the distribution function.

At the onset of cavity growth, all cavities are approximately of the same size, containing three vacancies and three helium atoms. As irradiation proceeds, these critical HeVCs diffuse and drift in the h-v phase space. Figure 13 shows the evolution of the size distribution of HeVCs at various irradiation times. Note the broadening of the distribution function with time. Figure 14 shows the results of the HeVC size distribution as function of both helium and vacancy content at approximately 14 dpa of irradiation (corresponding to approximately 1.3×10^7 s for HFIR conditions). While the distribution is narrow for small clusters, it broadens as the peak traces out a path close to the trajectory. Although all previous analytical attempts have only been able to predict the trajectory path of the

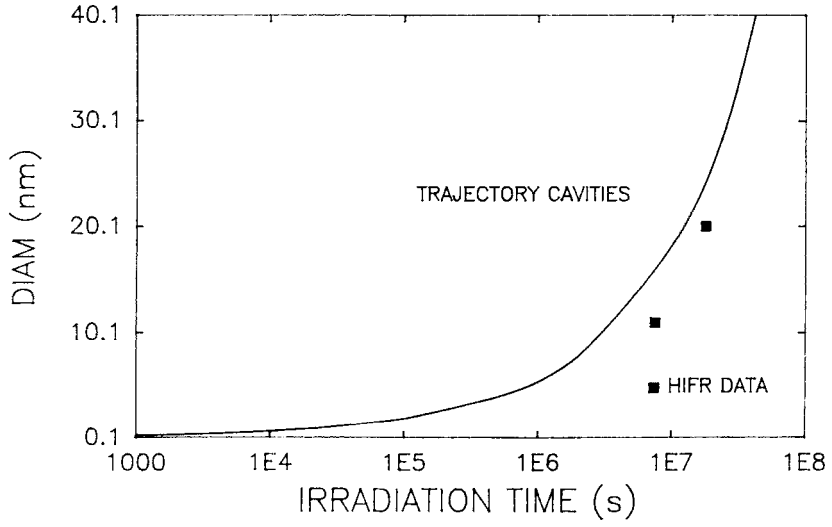

FIGURE 11 Time evolution of cavity size irradiated under HFIR conditions at 450°C as estimated by the trajectory method (data points [21]).

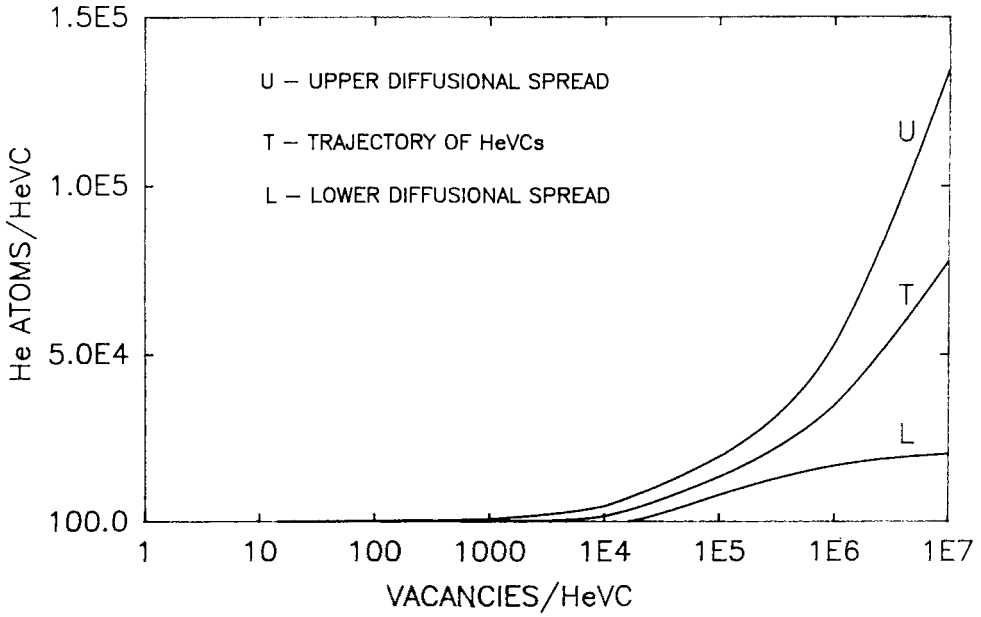

FIGURE 12 Growth trajectories of HeVCs for HFIR irradiation conditions using five times the estimated diffusional spreads.

HeVCs,[4] our model is the first one that establishes the transient size distribution function in the h-v phase space.

Figure 15 shows the dependence of the cavity distribution function on cavity diameter and helium content for HFIR irradiation conditions. At the onset of

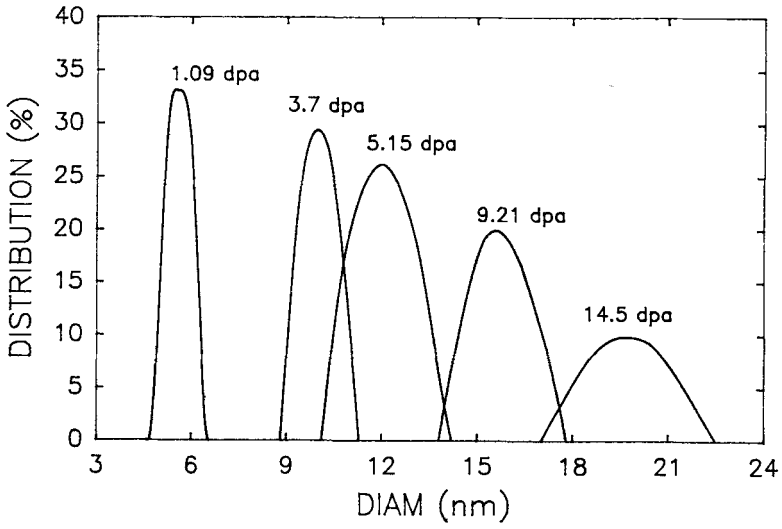

FIGURE 13 HeVC size distribution function at various irradiation times for typical HFIR irradiation conditions at 450°C.

growth (~ 0.1 dpa), there is a large concentration of small HeVCs (~ 2 nm/diam) containing between 100 and 200 helium atoms. As irradiation continues, the HeVCs grow in size to about 5 nm containing a few 100 to several 1000 helium atoms at 1.1 dpa. This evolution process is followed up to about 14 dpa (final experimental results). At that time, the average size is about 20 nm and may contain up to 3.5×10^4 helium atoms. Unfortunately there is no experimental data for the helium content distribution of cavities as a function of irradiation time and cavity size. The data available are only with respect to the size distributions.

To compare our model to experimental findings, the cavity concentrations are converted to distribution percentages. The results are shown in Fig. 16. The model predicts a narrower size distribution with the peak position roughly coinciding with experimental data.[21] The computed size distribution is shown to be narrower than experimentally observed. The spread of the distribution is solely dependent on emission/absorption probabilities, which govern the dispersion coefficient (**D**) in the F-P equation. We have not accounted for cascade effects on **D**. It is therefore consistent to conclude that cascade effects are significant on the spread of the distribution function.

7 SUMMARY AND CONCLUSIONS

A model was developed to account for transport, nucleation, and detailed evolution of HeVCs during irradiation. As such, it is the first model developed to encompass all stages of helium-filled cavity growth from atomistic sizes (few defects per HeVC) to macroscopic dimensions (containing up to 10^7 constituents per cavity). A detailed set of cluster-kinetic rate equations is set up to determine the nucleation rate of stable HeVCs during irradiation. One advantage of using the rate theory approach is that the effects of HeVC formation on the transport of helium

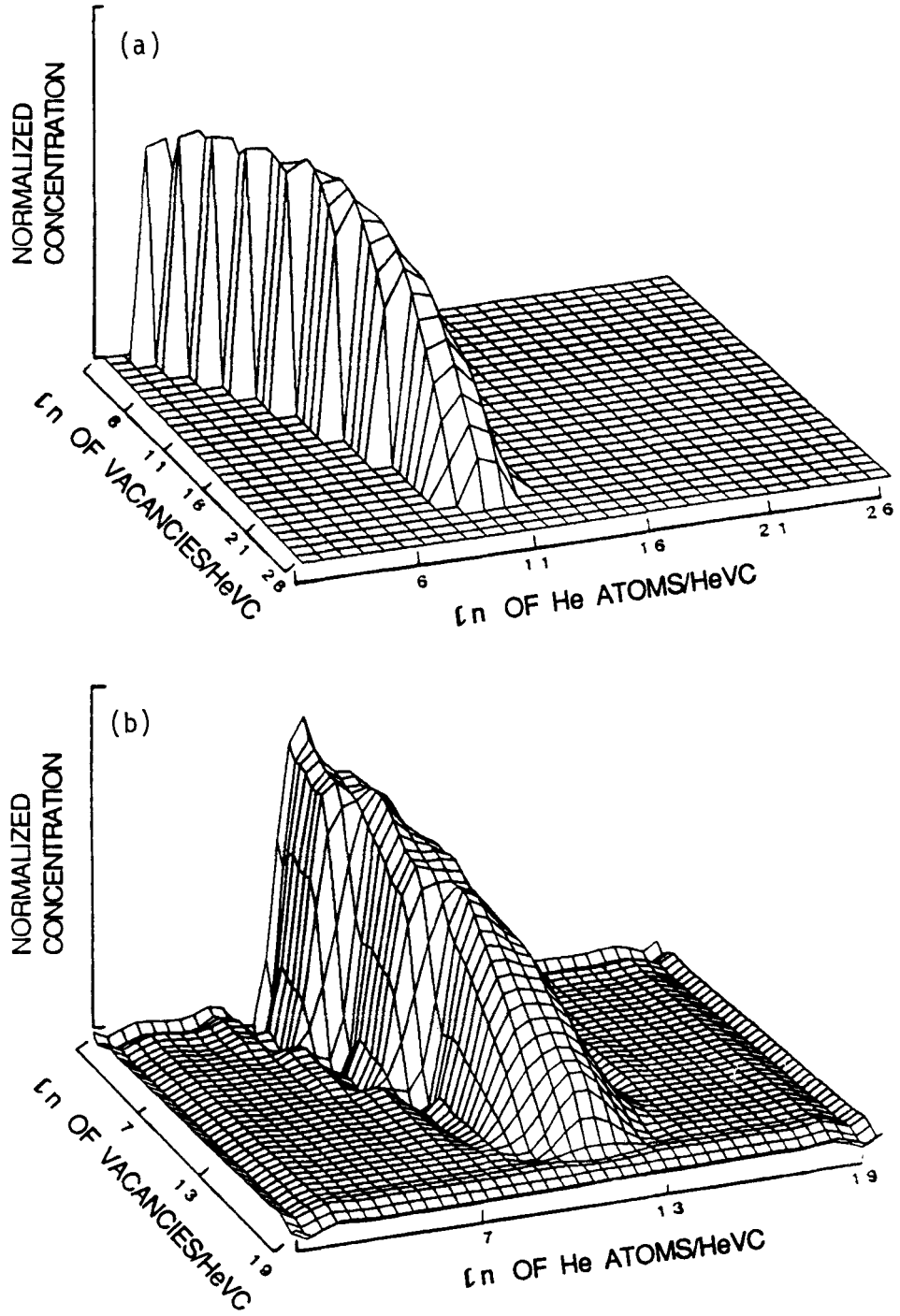

FIGURE 14 Cavity concentration at 14 dpa as a function of vacancy and He content for HFIR irradiation conditions at 450°C: (a) Entire distribution function; (b) Detail of the forward-moving distribution.

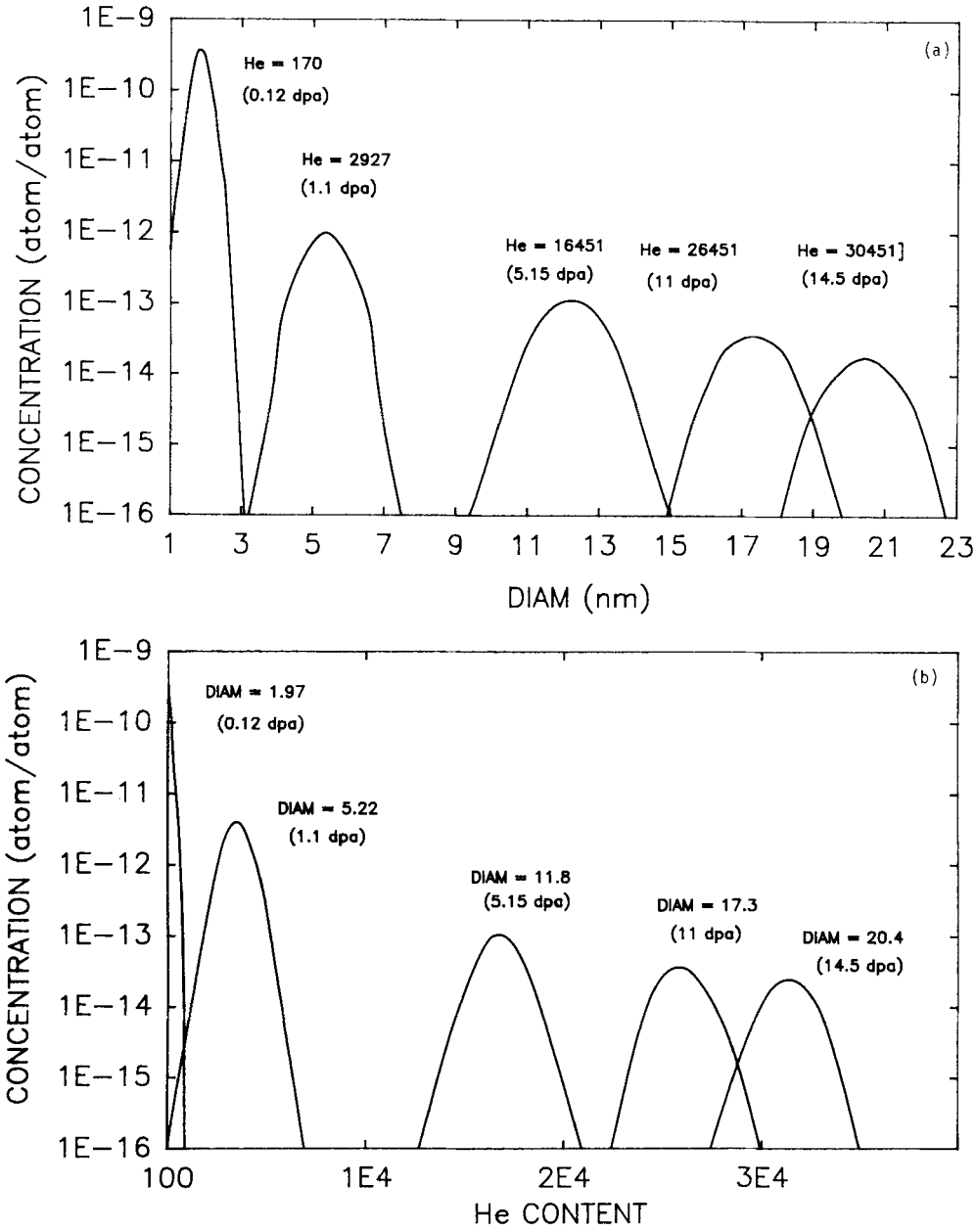

FIGURE 15 Cavity distribution function, for HFIR irradiation conditions at 450°C, at: (a) Avg He content as a function of diam; (b) Avg diam as a function of He content.

atoms, vacancies, and SIAs during irradiation is included. The effect of the developing microstructure on the nucleation current of stable HeVCs is thus automatically incorporated. A parametric study of temperature effects identified various kinetic processes responsible for (effective) helium-atom transport during irradiation. The nodal line analysis was used to determine the most probable

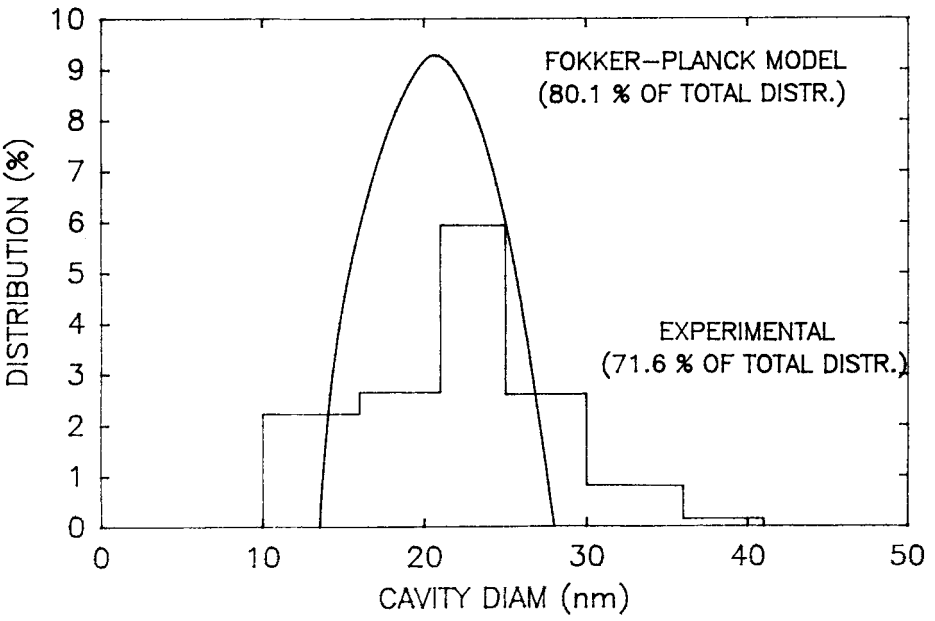

FIGURE 16 Comparison of computed and experimentally measured cavity size distribution at 14.3 dpa for HFIR irradiation conditions at 450°C (experimental data [21]).

combinations of helium atoms and vacancies in HeVCs as a function of time. In conjunction with the nodal line analysis, a virial expansion EOS was used to estimate binding energies of helium atoms and vacancies to h-v complexes as a function of cluster size and gas content.[7] Good agreement with atomistically calculated binding energies for small clusters was found. The effects of temperature, He/dpa ratio, re-solution of helium atoms, and material properties on the nucleation kinetics of HeVCs were investigated. Regions of spontaneous and stochastic nucleation conditions were established.

Starting with a general cluster kinetic master equation and taking moments of transition probabilities, we derived a continuum, 2-D (helium and vacancy content), time-dependent F-P equation. The F-P equation can be used to describe the growth of stable HeVCs into helium-filled cavities. However, the equation is too complex for analytical solution techniques. Therefore, a numerical approach was developed.

To solve the F-P equation in the h-v phase space, first a finite solution space was determined using a growth trajectory approach. Using the trajectory method, the average helium-filled cavity size and helium content can be estimated. Approximate diffusional spreads around the growth trajectory determine the boundaries of a minimum solution space for the F-P equation. A zero-current boundary condition across the boundaries of the solution space was set up. The advantage of this boundary condition is that the conservation principle can be invoked and erroneous numerical results are detected.

Finite differencing of the F-P equation and discretization of the solution space was used to develop a system of ODEs which were solved using the LSODE package. To model the growth of HeVCs, the system of ODEs must cover the range from stable nuclei (few defects per cluster) to macroscopic clusters containing up to

10^7 defects. To ensure the efficiency of the algorithm, a *dynamic re-meshing* method was developed. This algorithm fulfills two functions: (1) As the distribution of HeVCs drifts in the h-v phase space towards larger cluster sizes, the solution space follows (dynamically) the distribution movement (only equations which represent sizes in the vicinity of the distribution peak are solved). (2) Growth of the HeVCs is accompanied by dispersion of the size distribution in the h-v phase space [as the distribution broadens the mesh spacing is automatically increased (re-meshing)]. Using the dynamic re-meshing algorithm, the maximum number of ODEs being solved at any time was not more than 120 and typical computer runs used only 3 to 7 minutes of computation time on the CRAY-1.

The model was applied to Type-316 stainless steel exposed to typical HFIR irradiation conditions at 450°C up to about 14 dpa. This example was chosen because of the available experimental data base and because the high He/dpa ratio promotes spontaneous nucleation of HeVCs. Reasonable agreement between experimental and numerical results were found. In particular, at 14 dpa the peak of the calculated helium-filled cavity bubble size distribution coincides with measured values. However, the numerical size distribution is somewhat narrower than the experimental one. This is because cascade stochastic processes have not yet been included in our model. Such processes would lead to a further broadening of the calculated size distribution. Because our model uses a 2-D F-P equation (size and helium content), the helium content distribution is also evaluated. However, experimental data on the history of the helium content distribution in HeVCs is not yet available.

ACKNOWLEDGEMENT

This work was supported by the U.S. Department of Energy, Office of Fusion Energy, Contract # DE-FG03-84ER52110, with UCLA. The authors would like to acknowledge valuable discussions with Dr. H. Trinkaus.

REFERENCES

1. H. Trinkaus, *Radiat. Eff.* **78,** 189 (1983).
2. J. von den Diersch and P. Jung, *High Temperatures—High Pressures*, **12,** 635 (1980).
3. R. Manke, W. Jager, H. Trinkaus *et al.*, *Solid State Comm.* **44**(4), 481 (1982).
4. W. Jagar, R. Manzke, H. Trinkaus *et al.*, *J. Nucl. Mater.* **111/112,** 647 (1982).
5. W. G. Wolfer, in *Proc. 10th Conf. on Effects of Radiation on Materials*, ASTM STP 725, David Kramer, H. R. Brager and J. S. Perrin (Eds.) (Am. Soc. Testing Mater., Richland, WA, 1981), p. 201.
6. N. M. Ghoniem, S. Sharafat, J. M. Williams, and L. K. Mansur, *J. Nucl. Mater.* **117,** 96 (1983).
7. S. Sharafat and N. M. Ghoniem, *J. Nucl. Mater.* **122**(1-3), 531 (1984).
8. D. J. Reed, *Radiat. Eff.* **31,** 129 (1977).
9. H. Wiedersich, J. J. Burton, and J. L. Katz, *J. Nucl. Mater.* **51,** 287 (1974).
10. H. Wiedersich and B. O. Hall, *J. Nucl. Mater.* **66,** 187 (1977).
11. B. L. Eyre and R. Bullough, *J. Nucl. Mater.* **26,** 249 (1968).
12. B. O. Hall, in *Proc. 10th Conf. on Effects of Radiation on Materials*, ASTM STP 725, David Kramer, H. R. Brager and J. S. Perrin (Eds.) (Am. Soc. Testing Mater., Richland, WA, 1981), p. 512.
13. B. T. M. Loh, *Acta Metall.* **20,** 1305 (1972).
14. K. C. Russell and D. H. Hall, *Nucl. Metall.* **18,** 545 (1973).
15. K. C. Russell, *Acta Metall.* **26,** 1615 (1978).
16. W. D. Wilson, C. L. Bisson, and M. I. Baskes, *Phys. Rev. B*, **24,** 5616 (1981).
17. G. Nicolis and I. Prigogine, *Self-Organization in Nonequilibrium Systems* (Wiley, NY, 1977).
18. N. Wax, *Selected Topics in the Theory of Noise and Stochastic Processes* (Dover, NY, 1954).
19. A. C. Hindmarsh, "ODEPACK, a systematized collection of ODE solvers," in *Scientific Computing*, R. S. Stepleman *et al.* (Eds.) (North-Holland, Amsterdam, 1983).

20. H. Trinkaus, lecture notes at UCLA, July 1984).
21. P. J. Maziasz, "Effects of helium content on microstructural development in type-316 stainless steel under neutron irradiation," Ph.D. thesis, University of Tennessee, Knoxville (December 1984).
22. G. Farrell and W. A. Grant, *Radiat. Eff.* **3,** 249 (1970).
23. R. I. Cucker, K. Lakatos-Lindenberg, and K. E. Shuler, *J. Stat. Phys.* **9,** 2 (1973).
24. J. E. Inglesfield and J. B. Pendry, *Philos. Mag.* **34**(2), 205 (1976).
25. D. L. Johnson and J. R. Cost, in *Proc. Conf. on Defects and Defect Clusters in B.C.C. Metals and Their Alloys,* National Bureau of Standards, Gaithersburg, MD, August 1973, p. 279.
26. D. B. Poker and J. M. Williams, *Appl. Phys. Lett.* **40,** 851 (1982).
27. N. M. Ghoniem and S. Sharafat, "Numerical solution to the Fokker–Planck equation describing microstructure evolution," University of California Los Angeles Report No. UCLA-ENG-7962, 1979.
28. N. M. Ghoniem and D. D. Cho, *Phys. Status Solidi a,* **54,** 171 (1979).
29. P. J. Maziasz, *J. Nucl. Mater.* **103/104,** 987 (1981).